AFM nanomechanical properties and durability of new hybrid fluorinated sol-gel coatings

R. Suriano [a],[*], V. Oldani [b], C.L. Bianchi [b], S. Turri [a]

[a] Department of Chemistry, Materials and Chemical Engineering "Giulio Natta," Politecnico di Milano, Piazza Leonardo da Vinci 32, Milan 20133, Italy
[b] Department of Chemistry, Università degli Studi di Milano, via Golgi 19, Milan 20133, Italy

ABSTRACT

Microscopically homogeneous and thin fluorinated hybrid coatings showing significantly high mechanical and photochemical durability are prepared through the sol-gel chemistry and studied in this work. Their physico-chemical and nanomechanical properties are investigated. In this study, a special focus is given to the effects of organic/inorganic ratio and inorganic precursor type on surface and mechanical properties at the nanoscale. Different coatings containing low and high contents of silica as well as a mixed oxide composed of high amount of titania and low amount of silica are investigated. Nanoscratch and nanoindentation tests are performed by atomic force microscopy (AFM) and employed to assess the nanomechanical behavior of the hybrid coatings at a proper scale. Dynamic hardness results obtained from AFM are found to be in good agreement with technological pencil scratch tests performed at a macroscopic scale. Owing to the high inorganic content and good cross-linking degree achieved, coatings with a high amount of silica show considerably high dynamic hardness (nearly 2 GPa), which remains unchanged even after a long-term UV-vis light exposure. Notwithstanding the comparable inorganic amount, the hardness of mixed oxide coatings is markedly lower than high silica coatings and is subjected to modifications when exposed to UV-vis light in the long term, as also corroborated by x-ray photoelectron spectroscopy (XPS). Young's modulus results obtained by AFM nanoindentations appear to be dependent mostly on the inorganic/organic ratio. Higher moduli are determined for samples with higher inorganic/organic ratio, and no particular effect of the nature of inorganic precursor upon such property is observed.

© 2015 Elsevier B.V. All rights reserved.

1. Introduction

The study of mechanical properties of surfaces and coatings at the nanoscale has emerged as a key research topic over the last decade because it has enabled the analysis of mechanical performances of single-thin and complex multi-layer systems that cannot be otherwise investigated [1,2]. In this context, atomic force microscopy (AFM) has been increasingly used to evaluate nanoscratch resistance, elastic modulus and indentation hardness, owing to its capability to apply controlled loads of less than 100 μN [3,4]. This order of magnitude of the applied loads results in penetration depths of the order of 0.1 μm, allowing to assess surface mechanical properties of coatings without interference by the substrate. Moreover, by employing AFM to perform in situ topographical analysis of plastic deformations previously induced on surfaces, it is possible to gain a better understanding of mechanical behavior of films under investigation [5,6].

Organic/inorganic hybrid coatings are becoming increasingly used in many manufacturing sectors due to their ability to combine synergistically high durability, scratch resistance and surface cleanability [7–9]. Actually, by a careful co-formulation of different organic and inorganic components and by controlling their mutual arrangement, it is possible to develop innovative materials with remarkable properties and performances, which cannot be found in the single component coating. In addition to the ease of preparation and handling, organic/inorganic hybrid coatings possess a high optical transparency, mainly due to good homogeneity of final products at the nanoscale, resulting from the interpenetration of the inorganic and organic domains, which can be also covalently bonded with each other [10]. More specifically, organic/inorganic materials can be classified in two broad classes: (1) class I which includes hybrid systems where organic and inorganic phases interpenetrate each other with weak interactions such as Van der Walls, hydrogen bonding or electrostatic interactions and (2) class II where the two phase are strongly bonded by covalent or iono-covalent bonds [11]. Owing to this transparency and ease of processing, they are frequently used as coatings for corrosion protection [12,13], showing high mechanical strength, abrasion and hardness resistance [14,15]. The inorganic precursors are responsible for the superior mechanical properties, mostly endowing hybrid coating layers with hardness and thermal stability [16]. On the other side, the presence of organic moiety generally provides

* Corresponding author. Tel.: +39 0223993249; fax: +39 0270638173.
E-mail address: raffaella.suriano@polimi.it (R. Suriano).

flexibility, toughness, film forming ability, and prevents the material from the risk of crack formation, which normally occurs in relatively thick, completely ceramic coatings.

Hybrid organic–inorganic coatings have been widely prepared through sol-gel process, which is a synthetic pathway historically used for the preparation of ceramic or glassy materials. More recently, this chemistry has been addressed to the synthesis of organic/inorganic hybrid composites. The typical sol-gel precursors are silicon and metal alkoxides of the type $(RO)_x$-M, that through hydrolysis and condensation reactions lead to the formation of an inorganic M-O-M network within the organic matrix. Among the most frequently used inorganic precursors there are silicon alkoxides [17], but much attention has been also paid to organic–inorganic hybrids involving titania–silica mixed oxides as inorganic components [18,19]. These mixed oxides have attracted significant research interest, because of their wide range of applications, such as glasses with high strength [20], formation of super-hydrophilic and self-cleaning surfaces [21,22], and heterogeneous catalysts [23,24]. However, many previous works [25–27] showed that the addition of high reactivity titanium alkoxides in the sols causes some problems in the synthesis of the hybrid composites. Metal alkoxides possess high reactivity towards hydrolysis and condensation making difficult the sol-gel reactions in combination with the lower reactivity silica alkoxides without undesirable phase separation. The common way to sort this problem out is to introduce chelating agents [25–27], which limit the reactivity of metal alkoxides by complexation with the metal. However, the introduction of chelating agents can decrease the degree of cross-linking of the gel network, due to the smaller proportion of hydrolysable OR groups. Typical preparations of titania–silica mixed oxides, without the use of any complexing agent, consist of the pre-hydrolysis of silica precursors followed by the slow addition of titania precursors diluted in solvent in acidic conditions [28]. It has been reported that, for mixed TiO_2–SiO_2 oxides, a low H_2O/Ti alkoxide ratio must be maintained in order to minimize the rapid precipitation and the homocondensation of titanium alkoxides and to favor the increase of gelling time which promotes Ti-O-Si linkage formation [27].

In this study, nanoscratch hardness and Young's modulus of new fluoropolymer-based organic/inorganic hybrid coatings were investigated by means of AFM nanoscratch and nanoindentation tests, respectively. A hydroxyl-functional fluoropolymer binder belonging to the series of chlorotrifluoroethylene-vinylether copolymers was selected for this purpose, considering the distinctive properties of this polymer such as its easy handling as well as excellent weather resistance, good adhesion, hardness and flexibility of coated film [29]. This copolymer was thus functionalized with an isocyanate-functionalized silane to covalently bond the organic resin to the inorganic domains. Silica oxide was the inorganic component of choice for this work, because silicon alkoxides were considered particularly suitable for enhancing the co-cross-linking between the inorganic content and the functionalized organic resin. In fact, Si alkoxides enable the occurrence of a sol-gel reaction between the silanized fluoropolymer and alkoxysilane groups and this consequently can improve mechanical properties, chemical resistance and weathering resistance. In addition, a transition metal alkoxide (i.e. titanium isopropoxide) with an atomic number of metal higher than silicon was selected in order to evaluate the influence of inorganic Ti-O-Si and Ti-O-Ti networks on hybrid coatings hardness, scratch resistance and mechanical properties. To minimize undesired phase separation of titanium oxide from sols, two different pre-hydrolized precursor solutions were prepared separately and then added to the organic binder once hydrolyzed. As previously demonstrated in a previous study by our group [30], the SiO_2–TiO_2 hybrid fluorinated coatings were found to show a photocatalytic activity and super-hydrophilic behavior upon UV exposure, even in presence of fluoropolymer phase. As opposed to previous work, the effect of the inorganic content and the type of inorganic alkoxides on the nanomechanical properties of fluorinated hybrid coating were investigated in the present study. In

addition, the effect of long-term UV light exposure (over 500 h of UV-vis light irradiation in a weather-o-meter) on nanomechanical properties and coating surface composition was investigated to assess the durability of the hybrid coatings, even in presence of photoactive titanium oxide phases.

2. Experimental Part

2.1. Materials

The inorganic precursors tetraethylorthosilicate (TEOS), titanium isopropoxide (TIPT), ethyl acetate (AcOEt), high-purity water (CHROMASOLV® Plus, for HPLC) and hydrochloric acid (HCl 37 wt%, density (20 °C) $\geq$ 1.18 g/ml)) were supplied by Sigma Aldrich, Italy. Sulfuric acid, ACS reagent nominally 95–98 wt%, and H_2O_2 30 wt% (PERDROGEN™) were also purchased by Sigma Aldrich, Italy. The (3-isocyanatopropyl)triethoxysilane (IPTES) and dibutyltin dilaurate (DBTDL) were both purchased from Fluka, Switzerland. The fluorocarbon resin Lumiflon LF-910 LM is a chlorotrifluoroethylene-vinylether copolymer (FEVE in the following) provided by Asahi Glass, Japan, and it was used as a starting fluoropolymer binder for the following functionalization steps [31]. All the products were used without any further purification.

2.2. FEVE functionalization

The functionalization of FEVE with IPTES was carried out in a three-necked flask equipped with thermometer, reflux condenser and nitrogen gas inlet system. 40 g of FEVE (dry content 26.4 g, 0.047 hydroxyl equivalents) were loaded after a nitrogen flux was streamed into the flask for 5 min to eliminate the residual moisture and the temperature was increased to 75 °C. Then, IPTES (3.5 g, 0.014 isocyanate equivalents) was added to the fluoropolymer.

After 10 min of stirring, a solution of DBTDL (diluted to 1 wt% in AcOEt) was introduced into the mixture so that the DBTDL content was 0.03 wt% with respect to the FEVE dry content. The progress of the reaction was monitored by FTIR for evaluating the disappearance of the NCO adsorption band (NCO stretching, 2260 cm^{-1}). FTIR spectra were obtained with a Thermo Nicolet FTIR NEXUS SC-74 apparatus. It was found that under these experimental conditions, the reaction was completed within 4 h (Scheme 1). After this time, no more NCO groups were detected, meaning that they all have reacted with the OH groups. The final product was diluted with EtOH up to 50 wt%. One-third of the existing OH groups were end-capped with IPTES as the best trade-off between silanized resin shelf-life and compatibility with inorganic sols. The functionalized fluoropolymer was called FEVEsil in the following.

2.3. Preparation of the organic–inorganic hybrid sols

SiO_2/TiO_2 hybrid coatings were prepared by using the sol-gel method. The formulations containing mixed oxides involved a different procedure than those containing SiO_2 alone. As an example, for the coating with a higher silica content, the FEVEsil resin (1 g), the Si alkoxide (3 g, 0.014 mol) and the EtOH (3 g, 0.065 mol) were separately prepared and mixed together, and then water/HCl (0.1 g, 0.001 mol of HCl 37 wt%, diluted in 0.9 g, 0.05 mol of water) was added, following a magnetic stirring at room temperature for 1 h. The molar ratio used was TEOS:EtOH:H_2O:HCl = 1:4.5:3.5:0.07. The SiO_2/TiO_2 hybrid formulation was prepared by mixing the two precursors sols (TEOS and TIPT) after a separate pre-hydrolysis of the corresponding alkoxides. The TEOS solution was prepared by diluting TEOS in EtOH and then adding a solution of H_2O and HCl 37 wt% under magnetic stirring at room temperature. The molar ratio are the following: TEOS:EtOH: H_2O:HCl = 1:2.7:2.2:0.2. The TIPT solution was prepared in the same way by dissolving TIPT in EtOH and adding a solution of H_2O and HCl
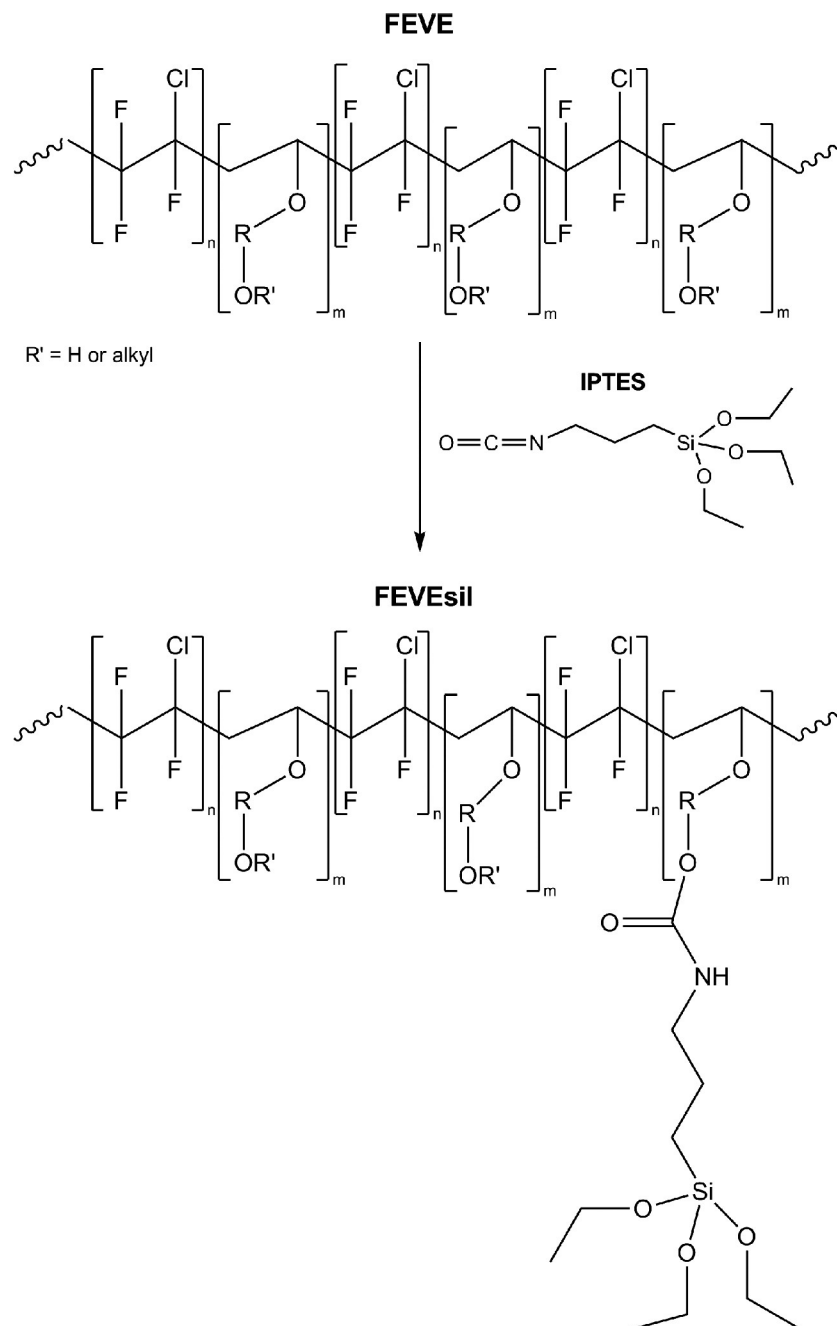
Scheme 1. Chemical reaction of FEVE resin with IPTES in order to obtain the silanized organic resin FEVEsil.

37 wt% under magnetic stirring at room temperature. The molar ratio are the following: TIPT:EtOH:H_2O:HCl = 1:32:0.81:0.12. The two pre-hydrolyzed solutions were then mixed together according to the weight percentages reported in Table 1 and kept under magnetic stirring for 1 h before adding the FEVEsil resin. The final mixture was kept for 1 h under magnetic stirring before application. The theoretical SiO_2 content varied from 62.4 to 10 wt% (neglecting the small SiO_2 amount deriving from FEVEsil). All the formulations were bar applied onto well-cleaned glass substrates after 24 h from the preparation of the sols and cured at 150 °C for 1 h. The dry film thickness was found to be in the range of 1–5 μm.

2.4. Technological and physico-chemical characterization

Macroscopic scratch hardness (pencil hardness) and chemical resistance (MEK double rubs) tests were done according to ASTM

D-3363–92a and ASTM D5402-93, respectively. The coatings thickness was measured by optical profilometry (Microfocus, UBM), whose maximum vertical resolution is 6 nm and maximum detectable range 500 μm. DSC analysis was carried out with a Mettler Toledo DSC823® instrument with three consecutive thermal runs at a scan rate of 20 °C/min: (1) from 0 °C to 250 °C, (2) from 250 °C to 0 °C and (3) from

Table 1
Composition of all the organic–inorganic hybrid coatings, investigated in this work.

Sample	FEVEsil wt%	SiO_2 wt% (from FEVEsil)	SiO_2 wt% (from TEOS)	TiO_2 wt%
$Fs_{81}S_{19}T_0$	81.2	3.0	15.8	0.0
$Fs_{39}S_{11}T_{50}$	38.6	1.4	10.0	50.0
$Fs_{37}S_{63}T_0$	36.7	0.8	62.5	0.0

0 °C to 250 °C. The value of residual enthalpy ΔH_{res} was measured calculating the area underneath the endothermic peak recorded during the first heating run. The glass transition T_g was determined as the midpoint of the curve shift in the endothermic direction during the second heating run. More specifically, a range surely including the glass transition temperature, was reported in case of unclear determination of the midpoint. Contact angle measurements were performed at room temperature by means of the sessile drop technique with an OCA20 instrument (Dataphysics Co., Germany), equipped with a CCD photo-camera and with a 500 mL Hamilton syringe to dispense liquid droplets. Ultra-pure water was used as a probe liquid, and at least 10 measurements were performed at different locations on the surface of each sample and results were averaged. All hybrid coatings were subjected to weathering tests under continuous Xenon light illumination in a weather-o-meter chamber (Solarbox3000e, Cofomegra S.r.l.) equipped with an outdoor filter cutting all wavelengths below 280 nm. The total irradiance was measured by means of a power meter with thermopile sensor (Ophir) and found to be approximately 1000 W/m^2 (550 W/m^2 in the 300–800 nm wavelength range [32]). The UV light irradiance level in the 295–400 nm range was 50 W/m^2, as measured by means of a UV-photodiode. The surface composition of coatings was investigated by x-ray photoelectron spectroscopy (XPS) before and after weathering tests. The spectra were obtained using an M-Probe apparatus (Surface Science Instruments); the source was monochromatic Al Kα radiation (1486.6 eV). For each sample, survey analyses in the whole range of X-ray spectra were performed (0–1000 eV Binding Energy), the depth of investigation of the instrument was about 50 Å. The relative percent abundance of elements is measured on a 400 x 1000 μm^2 sample spot.

2.5. AFM nanoindentation measurements

All indentation tests were carried out with an AFM (NSCRIPTOR system) driven by SPMCockpit software (NanoInk., Skokie, IL) in ambient conditions (temperature T, which ranges from 20 to 23 °C and relative humidity (RH, expressed in %) from 30 to 40) using commercially available silicon ACT probes purchased from AppNano (Santa Clara, CA) with a nominal spring constant of 40 N/m. The actual value of spring constants was calculated with the Sader method [33]. In case of more hydrophilic coatings containing titania, the value of RH was decreased to 15% in order to avoid the occurrence of adhesion phenomena and to correctly apply the Sneddon model for the determination of elastic moduli from force–distance curves.

Each probe was calibrated by performing a force–distance curve on a silicon wafer substrate. Before the calibration, each silicon surface was cleaned by immersion for 30 min in piranha solution (1:3 mixture of H_2O_2 30 wt% and concentrated sulfuric acid) then rinsed with ultra-pure water, methanol and blown dry with nitrogen. Substrates were also cleaned ultrasonically in ethanol for 15 min and dried with a nitrogen flux. Force–distance curves were carried out by applying a voltage to the piezoelectric transducer and by moving at the same time the probe towards the surface. When the tip was approached to the substrate, pressed against it (loading phase) and then retracted (unloading phase), the cantilever deflection was recorded as a function of vertical displacement of the piezoelectric sensor. The force–distance curve consists of two parts: (1) the flat part corresponds to probe movement above the surface, without any cantilever deflection, and (2) the sloped part indicates deflection of the cantilever when pressed against the surface. The probe calibration procedure is necessary to calculate the optical cantilever sensitivity, which allows to convert the cantilever deflection from the value measured by AFM and given in mV into the value of deflection in nm. The deflection d of the cantilever is equal to the vertical extension z of the piezo-sensor on a sample with stiffness higher or comparable to that of probe ($d = z$). In case of softer

sample, the cantilever tip will indent the surface. From the approach part of the force curve, the indentation depth or deformation δ is obtained and defined by the following relation:

$$\delta = z\text{-}d \tag{1}$$

As a result of the indentation δ, soft sample will have a smaller deflection and a force–distance curve with a smaller slope when compared to stiff sample [34]. A silicon wafer substrate was used as a stiff sample for calibration because AFM silicon tips were chosen for these measurements. The sensitivity value was so obtained by calculating the slope of the linear part of the force–distance curve. This procedure was repeated every time the probe was replaced and the laser was re-focused on the cantilever, because the sensitivity depends on the optical path length of the laser and the laser position on the cantilever.

Hybrid samples were examined at least 30 days after their preparation and were blown dry with nitrogen before any measurements to remove contaminations from the surfaces. To acquire the force–distance curve in a position not already touched by the tip, the probe was lifted up and the tip was then moved to another place. Elastic modulus or apparent Young's modulus of samples under investigation was obtained from the force–distance curves based on the Sneddon model [35]. According to Sneddon, the relation between the deflection d and the indentation δ can be written as follows,

$$d = \frac{2}{\pi} \frac{E_s}{(1-\nu_s^2)} \frac{\tan\vartheta}{k} \cdot \delta^2 \tag{2}$$

where E_s is the elastic modulus of the coating (assuming an infinitely higher modulus of the probe compared to the sample), ν_s is its Poisson ratio that was considered to be equal to 0.2 for hybrid organic–inorganic coatings [36], ϑ is the half-opening angle of the silicon tip (~24° in our case according to SEM images obtained after indentations [37]) and k is the spring constant of probe cantilever. The value of Young's modulus was calculated by fitting the Sneddon model to the curves in the region of reversible elastic deformations according to the method developed in a previous paper [37].

2.6. AFM nanoscratch tests

To investigate surface hardness at the sub-micron scale, AFM nanoscratch tests were carried out with an NSCRIPTOR system using a Bruker DNISP nanoindentation probe, consisting of a diamond tip mounted on a stainless steel cantilever (calibrated spring constant certified by supplier $k = 195$ N/m). Nanoscratch tests were performed by applying an average normal load of 66 μN and 96 μN on the tip. These values of the applied force were calculated by calibrating the deflection sensitivity of the DNISP probe, thus acquiring a force–distance curve on a rigid sapphire sample with the procedure explained in the previous paragraph 2.5. Such values of applied loads were also selected in order to avoid to go deep into the coatings with a penetration depth higher than 10% of the thickness of the pristine samples. Nanoscratches were obtained using a lithographic software (Nanoink's InkCAD) and setting a scratch length of 14 μm and a scratching rate of 0.1 μm/s and 10 μm/s.

Dynamic hardness H_s was evaluated using the following equation:

$$H_s = \eta \frac{F}{w^2} \tag{3}$$

where η is a constant depending on the geometry of the tip, F the normal load applied and w is the width of the scratch groove (measured at the height level of the specimen baseline surface) [38]. In case of conical probe, η is equal to $8/\pi$, while the constant value is 4.786 for the nanoindentation probe used in this work [6]. Actually, the diamond

Table 2
Chemical resistance (MEK test), pencil hardness and static contact angle measured with water as a probe liquid θ_{H_2O}, thickness measured by profilometry, residual enthalpy ΔH_{res} and glass transition temperature T_g measured by means of DSC analysis.

Sample	MEK test	Pencil hardness	ΔH_{res} (J/g)	T_g (°C)	θ_{H_2O} (°)	Thickness (μm)
$Fs_{81}S_{19}T_0$	>100	2B-B	−4.08	35–40 broad	92.0 ± 2.0	4.1 ± 0.8
$Fs_{39}S_{11}T_{50}$	>100	B-2H	−69.28	147.43	89.2 ± 1.6	0.7 ± 0.2
$Fs_{37}S_{63}T_0$	>100	7H-8H	−29.87	144.40	90.5 ± 1.5	2.1 ± 0.4

tips is a pyramid with an equilateral triangular base and the value of η can be calculated by the following equation [6]:

$$\eta = \frac{4}{\sqrt{3}}\left(1 + \frac{\tan\beta}{\tan\alpha}\right) \tag{4}$$

where α (~45.5°) is the angle between the front edge and the axis of the pyramid and β (~47.5°) is the angle between the back face and the axis of the pyramid. The widths of nanoscratches were measured by acquiring images of nanoscratches in tapping mode using the ACT-SS probes purchased from AppNano (Santa Clara, CA). For each nanoscratch, different line profiles at various locations along the scratch were considered to measure at least 3 depths and widths, which were then used to obtain an average value of hardness. Line profiles were carefully selected in order to consider profiles distant from each other and from the starting and the ending scratch position. The values of hardness were then calculated and presented as an average of at least 4 measurements of nanoscratches performed on each sample.

3. Results and discussion

The aim of this work is to present a nanomechanical characterization of a new class of fluoropolymer-based hybrid sol-gel coatings [30], in the attempt to correlate mechanical properties measured at the nanoscale such as dynamic hardness and elastic modulus with physico-chemical properties of materials and results from macroscopic technological tests. Table 1 reports the nominal composition of the hybrid coatings considered in this work. For brevity, from here on the functionalized resin will be referred to as FEVEsil (please see also Experimental Part 2.2) and the coatings as $Fs_xS_yT_z$, where x, y and z are the weight percentage of the undiluted FEVEsil content, SiO_2 and TiO_2, respectively. Three different inorganic concentrations ranging from 19 to 63 wt% were analyzed in order to evaluate the effect of composition on nanomechanical properties and durability of the hybrid fluoropolymer coatings. Among them, a sol-gel coating with a high titania content (50 wt%) was included to assess the effect of the photoactive oxide phase on scratch resistance and durability toward photo-oxidation. The hybrid materials compositions reported in Table 1 were selected in order to investigate the effect of very different organic and inorganic contents on physico-chemical and nanomechanical properties of hybrid coatings. In case of comparable inorganic content, the influence of TiO_2–SiO_2 mixed oxide versus SiO_2 oxide in the coatings was also examined in this study. As shown in Figure S1 (Supplementary Material), where the characters behind the samples are clearly visible, optimal conditions for obtaining highly transparent and homogenous coatings after thermal curing were achieved for this study.

3.1. Pencil hardness, solvent resistance test, DSC analysis and wettability behavior

All the hybrid films, although very thin, showed a very high chemical resistance evaluated by MEK rubbing tests (Table 2), confirming the formation of a highly interconnected organic/inorganic network. The results of pencil scratch tests showed in Table 2, however, reveal a big difference among the three coatings examined in this paper. Samples with a lower inorganic percentage ($Fs_{81}S_{19}T_0$) exhibited a quite poor scratch resistance as shown by the pencil hardness test value, around B. Sample $Fs_{37}S_{63}T_0$ on the opposite shows exceedingly high scratch hardness (7H-8H), with values normally not achievable by standard polymer coatings. Pencil hardness is lower for the sample containing a 50 wt% of titania. Accordingly, it is evident that the amount of silica phase plays a key role in providing significant scratch hardness to hybrid coatings because hard and rigid inorganic network can resist penetration of a pencil acting as an indenter during scratching process and therefore restricts plastic deformation of coatings. Notwithstanding the comparable inorganic fraction, $Fs_{39}S_{11}T_{50}$ coating shows lower pencil hardness than $Fs_{37}S_{63}T_0$, probably due to the presence of residual or partially reacted alkoxides in the mixed SiO_2/TiO_2 oxide sample, as indicated by higher residual enthalpy ΔH_{res} (Table 2). This suggests that the sample containing 50 wt% of titania possesses a lower cross-linking degree that provides its network with a less compact structure and thus a less scratch resistance.

The values of residual enthalpy and glass transition temperature measured by DSC were also reported in Table 2. Residual enthalpy is an indirect indication of the real extent of cross-linking of sol-gel coatings, being related to the evaporation of the polycondensation by-product. $Fs_{81}S_{19}T_0$ coatings showed a much lower value of residual enthalpy compared to the other samples. This may be certainly due to the lower density of cross-linking for coatings with a low inorganic fraction (SiO_2) that facilitates the complete evaporation of by-products during the heating post-treatment. Coatings with higher ceramic phase content show higher residual enthalpies, indicating that a part of the by-product is not completely evaporated during the curing step, or that some unreacted end groups still exist. This evidence is further corroborated by the quite high T_g values measured for $Fs_{39}S_{11}T_{50}$ and $Fs_{37}S_{63}T_0$ coatings, approaching the process temperature (140–150 °C). Moreover, we cannot exclude that residual hydroxyl groups, still present in FEVEsil, may condense with the alkoxides groups.

Table 3
Atomic abundance obtained by measuring the relative intensities of XPS emission from different species for all the organic–inorganic hybrid coatings investigated in this work before and after 527 h of light exposure in weather-o-meter chamber; two different values showed for $Fs_{39}S_{11}T_{50}$ sample before UV exposure are obtained from replicate measurements.

Sample	F (at %)		Si (at %)		Ti (at %)		O (at %)		C (at %)		Cl (at %)	
Light exposure (h)	0	527	0	527	0	527	0	527	0	527	0	527
FEVEsil	25	n/d	2	n/d	0	n/d	11	n/d	58	n/d	4	n/d
$Fs_{81}S_{19}T_0$	13	13	15	18	0	0	28	34	39	31	5	4
$Fs_{39}S_{11}T_{50}$	4; 8	0.1	11; 7	10	5; 6	19	40; 32	51	35; 44	20	2; 3	0
$Fs_{37}S_{63}T_0$	11	13	20	19	0	0	30	38	37	26	4	4

Static contact angles were measured using water as a probe liquid to examine the wettability behavior of these hybrid surfaces. Although the organic phase consists of a fluorocarbon resin, rather low water contact angles of nearly 90° were measured for all the coatings, which cannot be therefore considered very hydrophobic. This was actually to be expected because the pristine fluorocarbon polymer had a moderately low surface, due to the presence of polar C-Cl bond in the backbone. This feature of the resin was actually exploited with the aim of achieving photo-induced hydrophilicity for coatings containing photoactive TiO_2 phase generated *in situ* [30]. Moreover, the values of water contact angles appear to be quite comparable to each other, indicating no evident effect of the organic/inorganic ratio upon the wettability behavior. This suggests that the increase in the concentration of organic phase do not seem to enhance the presence of fluoropolymer on the surface of coatings prepared for this study; however, it is evident that the fluorocarbon chain is not totally embedded in the bulk of the coating.

3.2. X-ray photoelectron spectroscopy

The relative surface composition of each organic/inorganic hybrid coating was investigated by XPS analysis (Table 3). In each sample, the signals related to the electrons emission of fluorine were observed, thus confirming the presence of the functionalized FEVEsil resin in the outer coating layer (Figures S2, S3, S4 and S5). However, comparing the atomic ratio C/F of the hybrid coatings with FEVEsil, we observed that the value for $Fs_{81}S_{19}T_0$ and $Fs_{37}S_{63}T_0$ coatings slightly increased when compared to FEVEsil (C/F values were 3.0, 3.7 and 2.2, respectively). In addition, the atomic ratio C/F increased to 8.8 in the hybrid coating $Fs_{39}S_{11}T_{50}$, characterized by the presence of both SiO_2 and TiO_2. We supposed that the higher C/F value for $Fs_{39}S_{11}T_{50}$ may be due to the low conversion of the coating containing mixed oxides (see Table 2 for residual enthalpies), therefore presenting a higher concentration of carbon-containing end groups. After replication of XPS analysis, a
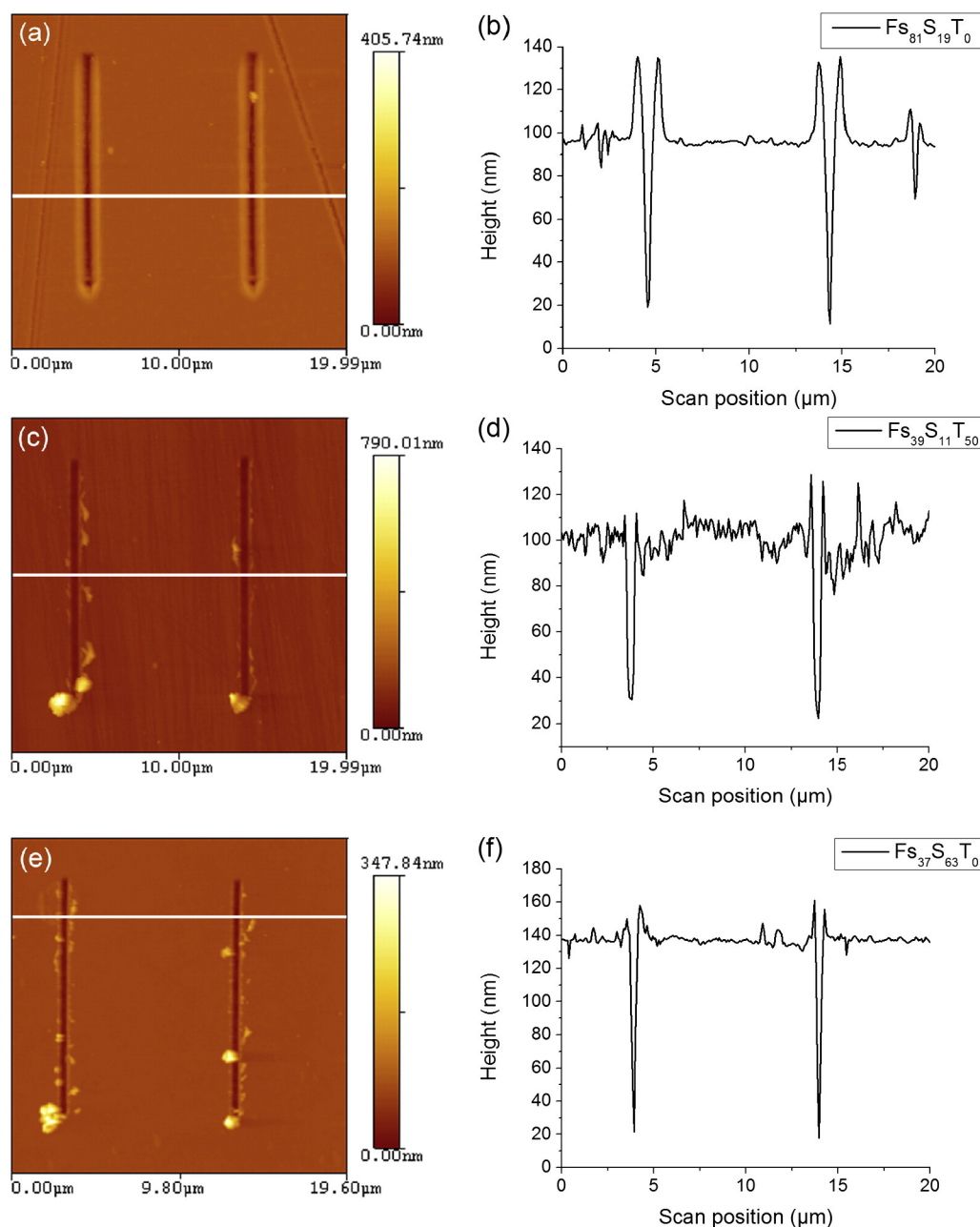
Fig. 1. AFM topographic images and transverse profiles of nanoscratches performed on the sample $Fs_{81}S_{19}T_0$ (a and b, respectively), $Fs_{39}S_{11}T_{50}$ (c and d, respectively) and $Fs_{37}S_{63}T_0$ (e and f, respectively) before light exposure in weather-o-meter chamber at a rate of 10 μm/s and applying a force of 66 ± 1 μN.

different C/F ratio of 5.5 was found just for $Fs_{39}S_{11}T_{50}$ (Table 3), suggesting the presence of a variability for this coating, probably due to residual non-reacted alkoxide groups. A photodegradative effect of titanium dioxide on this coating was also observed after the UV light exposure of the samples in the weather-o-meter chamber. After 527 h of light exposure, the C/F ratio of $Fs_{39}S_{11}T_{50}$ sample increased to 190, while the Ti/F ratio increased from 1.25 to 180. This suggests that the exposure of the photoactive coating to UV light led to a degradation of the polymeric component of the coating. Also, a surface enrichment in the more polar inorganic phases cannot be excluded (the hybrid surface containing mixed oxides becomes hydrophilic upon UV light exposure). On the other hand, for $Fs_{81}S_{19}T_0$ and $Fs_{37}S_{63}T_0$ coatings, the C/F ratio slightly decreased from 3 to 2.4 and from 3.7 to 2, respectively, after the light exposure.

3.3. Nanoscratch behavior and indentation measurements

The effect of inorganic content on mechanical properties was investigated by nanoscratch tests, where the coating is scratched by employing a nanoindentation probe mounted on AFM. The nanoscratches obtained at a rate of 10 μm/s by applying an average force of 66 μN are shown in Fig. 1.

Figs. 1b, d and f show the transverse profiles of nanoscratches performed on all the coatings, and Figs. 1a, c and e display the corresponding AFM topographic images. There is an evident difference between the nanoscratches obtained on the coatings with a low inorganic fraction and those with high inorganic contents. For $Fs_{81}S_{19}T_0$ samples, the deformation mechanism resembles that of a plastic plowing material (Fig. 1a). There is no apparent brittle cracking, and the material has flowed around the nano-indenter during the nanoscratch test, forming a uniform groove with evident ridges at the sides of the grooves (Fig. 1b). As for coatings with high inorganic/organic ratio, although they still showed some plastic deformation mechanism, it is evident that the debris of the material were formed by the nanoindentation probe, and they were either detached or pushed to one side of the scratch (Figs. 1c and e). Ridges of plastically deformed material either were not present, especially for $Fs_{39}S_{11}T_{50}$ samples, or for $Fs_{37}S_{63}T_0$ coatings were produced to a lesser extent, when compared to $Fs_{81}S_{19}T_0$.
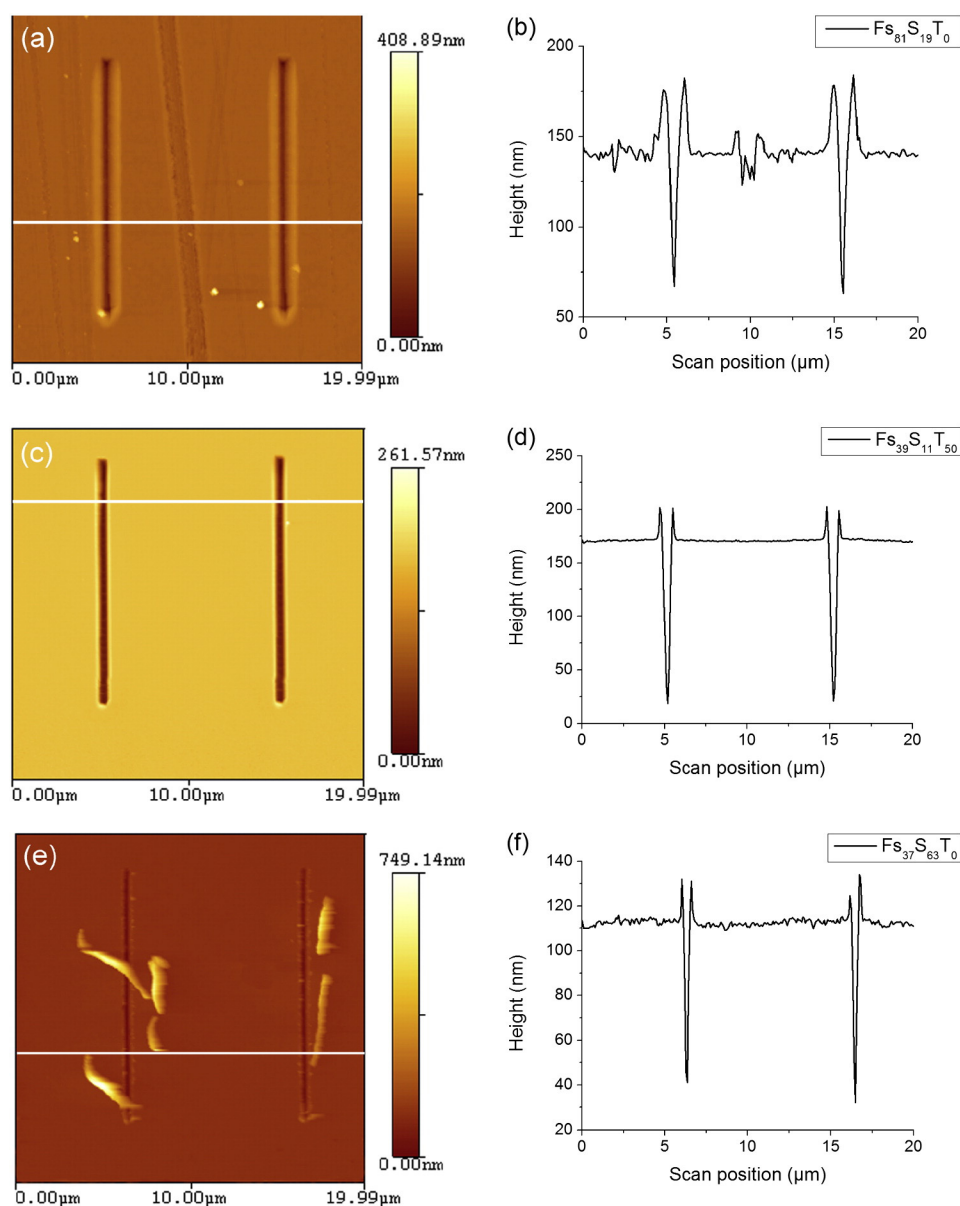
Fig. 2. AFM topographic images and transverse profiles of nanoscratches performed on the sample $Fs_{81}S_{19}T_0$ (a and b, respectively), $Fs_{39}S_{11}T_{50}$ (c and d, respectively) and $Fs_{37}S_{63}T_0$ (e and f, respectively) after 200 h of light exposure in weather-o-meter chamber at a rate of 10 μm/s and applying a force of 66 ± 1 μN.

When subjected to UV-vis light exposure (nearly 200 h of accelerated aging in weather-o-meter chamber), the deformation mechanism of coatings containing only silica appears rather similar to that of pristine material (Figs. 2a, b, e and f). On the contrary, for $Fs_{39}S_{11}T_{50}$ coatings, the behavior appeared to be one of a completely plastic plowing nature with measurable ridges formed at the sides of the groove (Figs. 2c and d). This can be probably related to the changes observed in the atomic abundance measured by XPS (Table 3). The decrease in the abundance of Cl and F after light exposure suggests that some photo-induced degradation of fluorocarbon polymer in presence of TiO_2 occurred in the first surface layers. This compositional change could have had an effect on the deformation mechanism during the nanoscratch tests, transforming the material behavior.

In order to analyze quantitatively the nanoscratch tests, an analytical model was considered to determine the scratch hardness, H_s, which is given by [38]

$$H_s = \frac{F_N}{A_{LB}} \qquad (5)$$

where F_N is the applied normal load and A_{LB} is the projected load bearing area, which is generally deduced from images of scratch width. According to the geometry of the indenter used in this study, the scratch hardness can be expressed by the Eq. (3). In this work, considering the high cross-linking degree of the hybrid coatings, it was assumed that the samples had a rigid-plastic behavior that typically supports the applied load only on the front face of the indenter. This is in contrast to the behavior of viscoelastic materials, which bear part of the normal load on the rear face of the indenter, due to the viscoelastic recovery of the material.

From the analysis of results in Fig. 3, it is evident that the coating containing the highest fraction of silica ($Fs_{37}S_{63}T_0$) shows a much higher dynamic hardness than the other two materials, which exhibit hardness of the same order of magnitude. In particular, the $Fs_{81}S_{19}T_0$ coating shows a value of dynamic hardness only marginally smaller than $Fs_{39}S_{11}T_{50}$. These results are in qualitative agreement with the trend of scratch hardness obtained from pencil tests (Table 2). By increasing the applied average load from 66 μN to 96 μN, the scratch hardness shows very little changes, which appear to be not significant considering the error bars (Fig. 3). The effect of the indenter rate during the scratch tests on hardness values was also evaluated. By comparing Figs. 4a and b, nanoscratch hardness before light exposure seems to be substantially unaffected by the indenter rate. However, unlike coatings with a high inorganic content, the $Fs_{81}S_{19}T_0$ coating exhibited a lower hardness by decreasing the probe rate. This might suggest that the nature of scratch deformation mechanism in these samples with the higher organic fraction is partially viscoelastic due to the dependence of scratch hardness upon the nanoscratch rate.
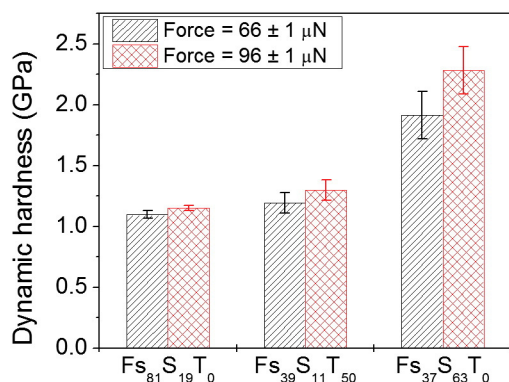

Fig. 3. Dynamic hardness of $Fs_{81}S_{19}T_0$, $Fs_{39}S_{11}T_{50}$ and $Fs_{37}S_{63}T_0$ coatings performed at a rate of 10 μm/s, applying a force of 66 ± 1 μN and 96 ± 1 μN by means of a diamond tip mounted on the AFM scanner.
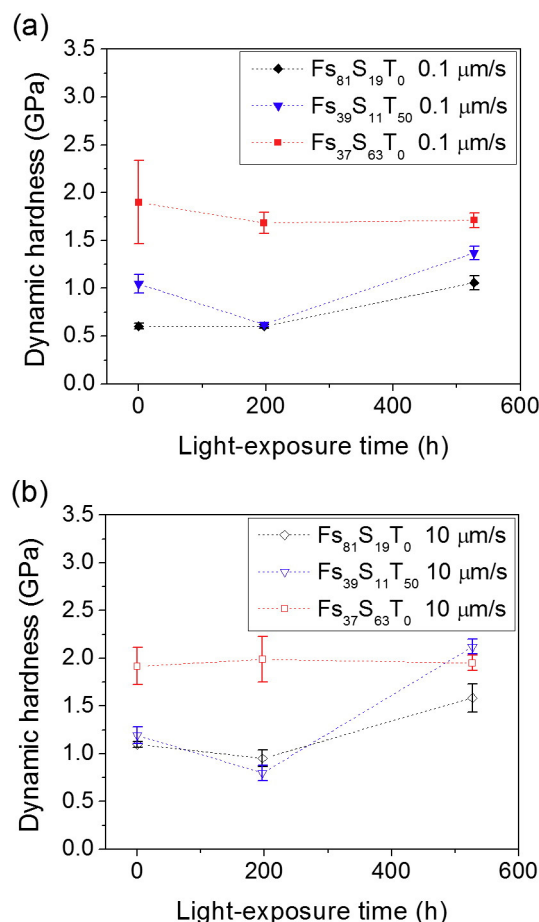
Fig. 4. Scratch hardness of $Fs_{81}S_{19}T_0$, $Fs_{39}S_{11}T_{50}$ and $Fs_{37}S_{63}T_0$ coatings performed at a rate of 0.1 μm/s (a) and 10 μm/s (b), applying a force of 66 ± 1 μN by means of a diamond tip mounted on the AFM scanner over light exposure time in a weather-o-meter chamber.

In order to evaluate the mechanical response of the hybrid coatings to weathering, nanoscratch tests were also performed after 200 h and 500 h of light exposure in a weather-o-meter chamber. As evident from Fig. 4, the coatings with the higher content of silica do not appear to undergo any significant changes upon the UV-vis light exposure. On the contrary, the coating containing titania shows an important decrease after 200 h of light exposure, followed by a remarkable increase after 500 h. This behavior can be attributed to the degradation of polymer binder photo-induced by the presence of TiO_2 or by a surface reorganization of more polar inorganic phases.

There is not a clear trend between the inorganic content of the coatings investigated and their nanoscratch depth (Fig. 5). In fact, all the penetration depths before light exposure are in the range of 60–130 nm, without any clear effect related to the inorganic percentage and the scratch speed. Among the coatings examined in this study, $Fs_{39}S_{11}T_{50}$ has the lowest nanoscratch depth. A correlation of scratch depths with elastic mechanical properties was previously reported in the scientific literature that studied scratching resistance of polymeric materials, where a higher scratch depth was associated with a reduction in the elastic modulus [39,40]. Taking into account also the results shown in Table 4 and discussed below, this correlation is not so evident for hybrid organic–inorganic coatings studied in this work. However, this can be explained by the scale of scratch depths, which are smaller than 200 nm in this work, but are typically in the μm scale in the literature. This indicates that, at nanometric scratch depths, the elastic modulus-related trend of scratch depths is less clear than at larger scale.

The results showed in Fig. 5c also reveal that the scratch deformed region on the $Fs_{37}S_{63}T_0$ surfaces do not undergo significant changes
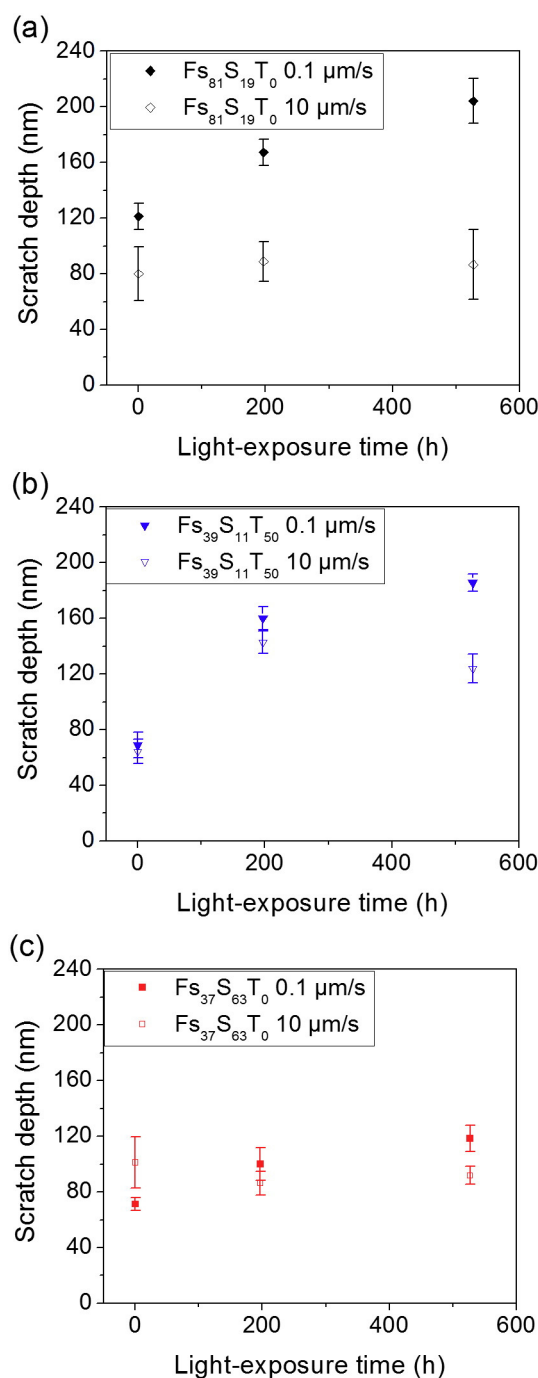
Fig. 5. Depth of the nanoscratches performed at a rate of 0.1 µm/s and 10 µm/s on $Fs_{81}S_{19}T_0$ (a), $Fs_{39}S_{11}T_{50}$ (b) and $Fs_{37}S_{63}T_0$ (c) coatings applying a force of 66 ± 1 µN by means of a diamond tip mounted on the AFM scanner over light exposure time in a weather-o-meter chamber.

upon prolonged light exposure for both the probe rates investigated. These results indicate that the coatings containing a high percentage of silica (63 wt%) exhibit a very good UV-vis light stability as well as a high scratch resistance, both on macroscopic and nanoscopic scale. On the contrary, after 500 h of light exposure, $Fs_{81}S_{19}T_0$ and $Fs_{39}S_{11}T_{50}$ coatings show an increase in the depths of nanoscratches performed at a rate of 0.1 µm/s (from 120 to 200 nm and from 70 to 190 nm, respectively). By employing a rate of 10 µm/s, only a smaller increase of scratch depths was observed after 500 h of light exposure for the sample containing titania (from 70 nm to 130 nm), while no evident increase was measured for $Fs_{81}S_{19}T_0$ coatings.

In order to quantitatively measure the Young's modulus for these hybrid coatings which are not self-standing films, AFM nanoscale indentation tests were also performed. Force vs. indentation curves were obtained for $Fs_{81}S_{19}T_0$ and $Fs_{39}S_{11}T_{50}$ surfaces using probes with similar characteristics, while a stiffer cantilever was needed to test $Fs_{37}S_{63}T_0$ samples. Cantilevers with a spring constant, which ranges from 30 to 40 N/m, and a pyramidal tip were selected for the nanoindentation of these moderately stiff materials ($Fs_{81}S_{19}T_0$ and $Fs_{39}S_{11}T_{50}$) [37]. By employing the Sneddon model to evaluate the elastic modulus (Eq. (2)), a remarkable difference of one order of magnitude in the elastic modulus of $Fs_{81}S_{19}T_0$ and $Fs_{39}S_{11}T_{50}$ coatings was measured (Table 4). Compared to $Fs_{39}S_{11}T_{50}$ samples, $Fs_{81}S_{19}T_0$ surfaces can be indented in a higher range of depths for comparable loads lower than 6 µN (Figs. 6a and b). Even by employing a stiffer cantilever ($k = 57$ N/m) to indent $Fs_{39}S_{11}T_{50}$ samples, similar values of indentation depth and elastic modulus were obtained (data not shown).

A difference between elastic moduli determined from forward and reverse curves is also evident for $Fs_{81}S_{19}T_0$, likely due to the partially viscoelastic nature of this coating, as already observed in the influence of nanoscratch rate upon the hardness value. In such cases, only the values determined from reverse curves are considered in order to minimize any contributions to the elastic modulus values from the viscoelastic deformation. The apparent discrepancy between nanoscratch and nanoindentation behavior obtained for $Fs_{81}S_{19}T_0$ and $Fs_{39}S_{11}T_{50}$ coatings can be explained by considering the different scale of loads and diverse type of deformations involved in these two experiments. For nanoscratch tests, forces ranging from 65 to 98 µN were applied, leading to plastic and permanent deformations of the samples. On the other hand, during AFM nanoindentation, the maximum load considered is approximately 10 µN in order to produce only elastic deformations. As for coating having higher content of silica, a stiff cantilever ($k = 63$ N/m) was used because softer probes did not provide any measurable indentation. Comparison of $Fs_{39}S_{11}T_{50}$ and $Fs_{37}S_{63}T_0$ samples indicates that the samples with mixed oxides but similar inorganic content have an elastic modulus comparable to samples with a single oxide. This could suggest that the bulk inorganic–organic composition has a predominant role in determining mechanical properties in the elastic region, such as Young's modulus, while the presence of different oxides could have a more relevant effect on scratch resistance.

4. Conclusions

The physico-chemical and nanomechanical properties of different fluorinated hybrid coatings were investigated at the nanoscale by varying the inorganic content and the type of inorganic precursors added in the sols. AFM nanoscratch tests show that the coating with a higher content of silica exhibits a remarkably high value of nanoscratch hardness of nearly 2 GPa, which is higher in comparison to the other coatings investigated. The values of nanoscratch hardness determined by AFM before the long-term light exposure also confirm the trend observed for the technological pencil hardness tests. In addition, nanoscratch tests indicate that, during the prolonged exposure to UV-vis light, scratch hardness does not significantly change for the sample with the higher

Table 4
Averaged maximum indentation ± coefficient of variation expressed in % (CV) and Young's modulus E_s ± standard deviation (SD) obtained using the Sneddon model for forward and reverse force curves measured on $Fs_{81}S_{19}T_0$, $Fs_{39}S_{11}T_{50}$ and $Fs_{37}S_{63}T_0$ coatings.

Sample	Curve	Indentation (nm) ± CV	E_s ± SD (GPa)
$Fs_{81}S_{19}T_0$	Forward	99 ± 25%	1.8 ± 1.5
	Reverse	54 ± 11%	6.4 ± 0.9
$Fs_{39}S_{11}T_{50}$	Forward	25 ± 8%	36.6 ± 6.7
	Reverse	23 ± 26%	34.5 ± 9.2
$Fs_{37}S_{63}T_0$	Forward	49 ± 26%	25.0 ± 5.6
	Reverse	56 ± 22%	16.4 ± 3.5
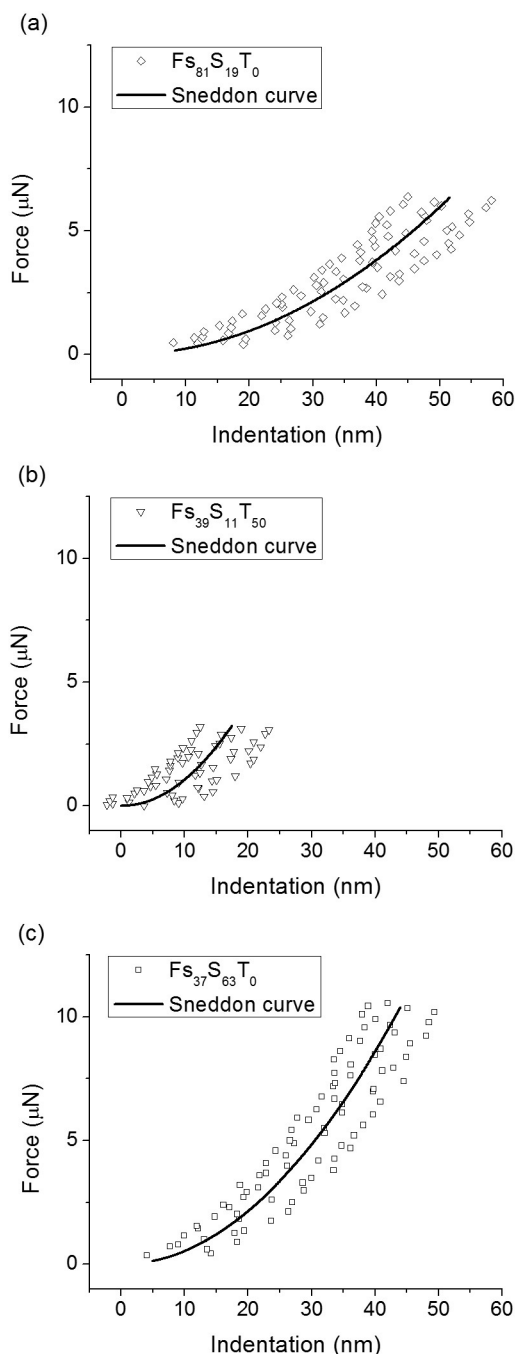
Fig. 6. Force vs. elastic indentation curve obtained from reverse phase with superimposed Sneddon model curve in the data set selected for $Fs_{81}S_{19}T_0$ (a), $Fs_{39}S_{11}T_{50}$ (b) and $Fs_{37}S_{63}T_0$ surfaces (c).

amount of silica, while the coating with mixed oxides may undergo a photo-induced degradation, likely owing to the photocatalytic effect of TiO_2 that deteriorates the polymeric phase, as also suggested by XPS analysis. By comparing samples with high and similar inorganic content, the difference in scratch hardness can be probably due to a lower cross-linking degree in the coating with mixed oxides. However, no significant differences in Young's modulus results are evidenced by AFM nanoindentation tests between the coatings with high inorganic fraction, which exhibit a value of modulus higher than samples with a lower inorganic content. Sample with 63 wt% of silica also provides a remarkable outdoor durability and therefore enables the improvement of mechanical properties of fluorinated hybrid coatings. The results of this study demonstrate that the use of AFM technique enables the mechanical characterization of inorganic/organic hybrid coatings at the nanoscale, showing their tribo-mechanical response, which can be significantly different from that at a larger scale. Moreover, this work offers a better understanding of structure-property relationships in such coatings so as to achieve the development of new hybrid coatings with enhanced durability and mechanical performances.

Acknowledgments

Appendix A. Supplementary data

Supplementary data to this article can be found online at http://dx.doi.org/10.1016/j.surfcoat.2015.01.015.

References

[1] C.A. Charitidis, Appl. Surf. Sci. 256 (2010) 7583–7590.
[2] A. Tiwari, L.H. Hihara, Surf. Coat. Technol. 206 (2012) 4606–4618.
[3] J.-C. Huang, C.-L Li, J.-W. Lee, Scanning 34 (2012) 51–59.
[4] B. Bhushan, Wear 251 (2001) 1105–1123.
[5] S. Turri, L. Torlaj, F. Piccinini, M. Levi, J. Appl. Polym. Sci. 118 (2010) 1720–1727.
[6] S. Graça, R. Colaço, R. Vilar, Tribol. Lett. 31 (2008) 177–185.
[7] B. Masheder, C. Urata, A. Hozumi, ACS Appl. Mater. Interfaces 5 (2013) 7899–7905.
[8] P. Fabbri, M. Messori, M. Montecchi, S. Nannarone, L. Pasquali, F. Pilati, C. Tonelli, M. Toselli, Polymer 47 (2006) 1055–1062.
[9] H. Yahyaei, M. Mohseni, Tribol. Int. 57 (2013) 147–155.
[10] O. García, L. Garrido, R. Sastre, A. Costela, I. García-Moreno, Adv. Funct. Mater. 18 (2008) 2017–2025.
[11] B. Samiey, C.-H. Cheng, J. Wu, Materials 7 (2014) 673–726.
[12] R.B. Figueira, C.J.R. Silva, E.V. Pereira, J. Coat. Technol. Res. 1–35 (2014).
[13] E. Roussi, A. Tsetsekou, A. Skarmoutsou, C.A. Charitidis, A. Karantonis, Surf. Coat. Technol. 232 (2013) 131–141.
[14] B. Ramezanzadeh, M. Mohseni, A. Karbasi, J. Mater. Sci. 47 (2012) 440–454.
[15] D.A. Banerjee, A.J. Kessman, D.R. Cairns, K.A. Sierros, Surf. Coat. Technol. (2014). http://dx.doi.org/10.1016/j.surfcoat.2014.07.091.
[16] Y. Sun, W. Liu, J. Mater. Sci. 47 (2012) 1803–1810.
[17] A. Ferchichi, S. Calas-Etienne, M. Smaïhi, G. Prévot, P. Solignac, P. Etienne, J. Mater. Sci. 44 (2009) 2752–2758.
[18] L. Chen, H. Shen, Z. Lu, C. Feng, S. Chen, Y. Wang, Colloid Polym. Sci. 285 (2007) 1515–1520.
[19] J. Zhou, M. Chen, X. Qiao, L. Wu, Langmuir 22 (2006) 10175–10179.
[20] S. Kirtay, E. Oktay, V. Gunay, Thin Solid Films 515 (2006) 2145–2152.
[21] S. Permpoon, M. Houmard, D. Riassetto, L. Rapenne, G. Berthomé, B. Baroux, J.C. Joud, M. Langlet, Thin Solid Films 516 (2008) 957–966.
[22] M. Houmard, D. Riassetto, F. Roussel, A. Bourgeois, G. Berthome, J. Joud, M. Langlet, Appl. Surf. Sci. 254 (2007) 1405–1414.
[23] W. Dong, Y. Sun, C.W. Lee, W. Hua, X. Lu, Y. Shi, S. Zhang, J. Chen, D. Zhao, J. Am. Chem. Soc. 129 (2007) 13894–13904.
[24] A.R. Oki, Q. Xu, B. Shpeizer, A. Clearfield, X. Qiu, S. Kirumakki, S. Tichy, Catal. Commun. 8 (2007) 950–956.
[25] U. Schubert, J. Mater. Chem. 15 (2005) 3701–3715.
[26] H. Schmidt, J. Non-Cryst. Solids 100 (1988) 51–64.
[27] H.S. Kibombo, R. Peng, S. Rasalingam, R.T. Koodali, Catal. Sci. Technol. 2 (2012) 1737–1766.
[28] Y.K. Kim, E.Y. Kim, C.M. Whang, Y.H. Kim, W.I. Lee, J. Sol-Gel Sci. Technol. 33 (2005) 87–91.
[29] T. Takayanagi, M. Yamabe, Prog. Org. Coat. 40 (2000) 185–190.
[30] F. Piccinini, M. Levi, S. Turri, Prog. Org. Coat. 76 (2013) 1265–1272.
[31] Asahi Glass Company, http://www.lumiflon.com/what_us/intro.html.
[32] Paints and varnishes—artificial weathering and exposure to artificial radiation—exposure to filtered xenon-arc radiationsecond ed., ISO 11341, 2004. (2004(E)).
[33] J.E. Sader, J.W.M. Chon, P. Mulvaney, Rev. Sci. Instrum. 70 (1999) 3967–3969.
[34] H.-J. Butt, B. Cappella, M. Kappl, Surf. Sci. Rep. 59 (2005) 1–152.
[35] I.N. Sneddon, Int. J. Eng. Sci. 3 (1965) 47–57.
[36] J. Malzbender, G. de With, Surf. Coat. Technol. 135 (2001) 202–207.
[37] R. Suriano, C. Credi, M. Levi, S. Turri, Appl. Surf. Sci. 311 (2014) 558–566.
[38] J.A. Williams, Tribol. Int. 29 (1996) 675–694.
[39] K. Friedrich, H.J. Sue, P. Liu, A.A. Almajid, Tribol. Int. 44 (2011) 1032–1046.
[40] C. Xiang, H.J. Sue, J. Chu, B. Coleman, J. Polym. Sci. B Polym. Phys. 39 (2001) 47–59.